Combust. Sci. and Tech., 182: 1341–1359, 2010
Copyright © Taylor & Francis Group, LLC
ISSN: 0010-2202 print/1563-521X online
DOI: 10.1080/00102201003694834

Taylor & Francis
Taylor & Francis Group

IGNITION BEHAVIOR OF α-AlH_3

G. Young,[1] N. Piekiel,[2] S. Chowdhury,[2] and M. R. Zachariah[2]

[1]*NSWC-Indian Head Division, RDT&E Directorate, Indian Head, MD, USA*

[2]*University of Maryland, College Park, MD, USA*

An experimental investigation on the ignition behavior of α-Aluminum Hydride (α-AlH_3) has been conducted. The ignition characteristics were determined through the use of two separate modified T-jump experiments. In each experiment, a small amount of material was placed onto a platinum wire, which was heated rapidly through resistive heating. As a result both ignition and hydrogen release temperatures were studied for heating rates ranging from 10^4 to 10^5 Kls. The hydrogen release temperature was determined in vacuum, and ignition was studied at ambient pressure in air, CO_2, and mixtures of argon with oxygen. Both the hydrogen release and ignition temperature increased as the heating rate increased. Hydrogen release temperatures ranged from approximately 650 to 1200 K, whereas ignition was observed to range from below the melting temperature of aluminum (933 K) to approximately 1500 K. Activation energies for hydrogen release were ~27 kJlmol, and are well below those reported by others at much lower heating rates. This result is consistent with the affects of higher heating rates transitioning the rate-limiting step from one of chemical kinetics to intraparticle hydrogen diffusion. For conditions in which the particles would ignite it was found that the environment did not play a significant role in the ignition temperature, beyond a critical oxygen mole fraction of $X_{O2} > 0.05$. Ensemble average burning times were found to decrease by a factor of about 3 when the oxygen mole fraction was increased from 0.1 to 0.5.

Keywords: Alane; Aluminum hydride; Decomposition; Ignition

INTRODUCTION

Alane is particularly interesting as an ingredient in fuels and propellants in propulsion systems because of its ability to substantially increase the performance of a given system. For instance, thermochemical calculations using the NASA CEA chemical equilibrium code indicate that replacement of aluminum with alane in a typical composite solid rocket propellant (Ammonium Perchlorate/HTPB/Aluminum) increases the specific impulse (I_{sp}) by ~7–8%. Furthermore, a substantially reduction in the adiabatic flame temperature is also expected. For example, at 90% solids loading, the highest performing alanized propellant has a flame

Received 8 April 2009; revised 14 December 2009; accepted 11 February 2010.
Address correspondence to M. R. Zachariah, University of Maryland, College Park, MD, 20742, USA. E-mail: mrz@umd.edu

temperature about 15% lower (3715 K with 25% Aluminum and 3158 K with 30% Alane) than the highest performing aluminized propellant. The reduced flame temperature suggests that less thermal protection would be required for a given rocket motor, resulting in improved mass fraction, meaning even further improvement in motor performance.

Although Alane is attractive as an ingredient in fuels and propellants, the primary reason that it has yet to make a major impact is that it exhibits poor thermal stability. There are as many as six crystalline phases of alane, the most stable of which, and the subject of this work, is α-alane (U.S. Patent No. 6,228,338, 2001). Although alane has been the subject of studies for more than 40 years very little information exists in the literature on its ignition and combustion behavior. Among the first published data on alane, Sinke determined the heat of formation as -2.7 kcal/mole by bomb calorimetry (Sinke et al., 1967). The decomposition of alane has been previously studied (see Bazyn et al., 2007; Ismail and Hawkins, 2005; Weiser et al., 2007), but typically at relatively low heating rates and relatively low temperatures. Graetz (Graetz and Reilly, 2005, 2006; Graetz et al., 2007) conducted a series of studies on the thermodynamics and decomposition kinetics of the different AlH_3 polymorphs and demonstrated that during decomposition, β and γ polymorphs transition to the α phase at about 100°C. Upon further heating, the α phase decomposes to H_2 gas and aluminum. For the temperature range conducted in their study ($60 < T\ [°C] < 160$), Graetz et al. (2005) determined that the kinetics of the hydrogen evolution from various aluminum hydride polymorphs were controlled by nucleation and growth of the aluminum phase.

Bazyn et al. (2007) measured the decomposition of alane by heating a small sample in a pressure vessel and monitoring the pressure increase. Under the conditions of their experiment, Bazyn et al. (2007) found that the hydrogen may be easily released from the particles at temperatures between 400–500 K. Ismail and Hawkins (2005) determined that alane decomposition proceeds in two steps: (a) a rate-limiting two-dimensional nucleation reaction and (b) growth of crystals. Ismail also determined that after the hydrogen is liberated from the particle, the resulting products are amorphous and crystalline aluminum.

Bazyn et al. (2004) proposed that in general combustion environments aluminum hydride would react via a two-step mechanism:

$$AlH_3 \rightarrow Al + \frac{3}{2}H_2 \quad \text{(dehydrogenation)} \tag{1}$$

$$Al + \frac{3}{4}O_2 \rightarrow \frac{1}{2}Al_2O_3 \quad \text{(oxidation)} \tag{2}$$

They studied the combustion of AlH_3 at high temperatures and pressures in a shock tube and concluded that the dehydrogenation step is significantly faster than ignition, and that once the hydrogen has been released the remaining aluminum burns similarly to aluminum of similar size (micron scale). In another study Il'in et al. (2001) studied the products of combustion of alane in air. Il'in et al. (2001) found that AlH_3 combustion in air had three stages: (a) a hydrogen flame, separated from the sample with a nonluminous zone; (b) a middle stage in which once the hydrogen was consumed, the flame descended and touched the sample resulting in

ignition and low-temperature combustion, similar to ultradispersed aluminum powder (UDAP); and (c) a high-temperature stage in which the sample reached 2000–2400°C. Il'in et al. (2001) analyzed the final combustion products and found a substantial amount of AlN content, which was consistent with previous studies on UDAP.

Although a limited amount of data is available for alane, there is a very large database available on the ignition and combustion behavior of aluminum in a wide variety of particle sizes, environments, and conditions. Unless specially treated, aluminum particles have a 2–5 nm oxide shell of Al_2O_3 surrounding the aluminum core. In order for ignition of the aluminum particle to occur, the oxide layer must be broken down to expose pure aluminum. According to Price (1983), the oxide layer can be broken down in two ways. First, because aluminum melts at a much lower temperature (933 K) than aluminum oxide (2327 K), the molten aluminum core expands, due to its lower density, and creates a thermal stress, and cracking in the oxide shell. Alternatively at sufficiently higher temperatures the oxide shell melts.

Friedman and Macek (1962, 1963) provided some of the earliest ignition data on aluminum. They found that ignition of aluminum particles (15–70 μm) only occurred at temperatures corresponding to the melting temperature of aluminum oxide (2300 K). Several other studies (see Brossard et al., 1997; Brzustowski and Glassman, 1964; Kuehl, 1965) found that the ignition temperature of various forms of aluminum ranged from approximately 2000–2300 K. Gal'chenko et al. (1973) studied the ignition of an aluminum wire in carbon dioxide and found that the ignition temperature of the wire also corresponded to the approximate melting temperature of aluminum oxide. On the other hand, Bazyn et al. (2006) observed that the ignition temperature of aluminum at the nanoscale is significantly lower than that of micron-sized aluminum, and as low as 1200 K.

EXPERIMENTAL APPROACH

The alane studied in this effort was α-alane (U.S. Patent No. 6,228,338, 2001), which is the most thermally stable form of aluminum hydride. The methods for synthesis and stabilization of the as received α-alane used in the study are not fully known to us, although it is likely to have been the same as the material studied by Ismail and Hawkins (2005), and Bazyn et al. (2004, 2007). Representative particles are shown in Figure 1 in an SEM image. The particles are rhombohedral crystals and range from a few microns to approximately 25 μm in size. In each of the subsequently described experiments, the alane was dispersed in hexane from which the samples were drawn into a syringe and then deposited on a platinum filament with a diameter of approximately 75 μm. Figure 2 is an SEM image of the alane deposited on the platinum filament. The samples were allowed dry in the ambient air prior to experiments.

Hydrogen Release Experiments

The hydrogen release kinetics were studied with a custom designed Temperature-Jump time-of-flight (TOF) mass spectrometer (Zhou et al., 2009a, 2009b). The T-jump system consisted of a ~76 μm diameter platinum wire, which

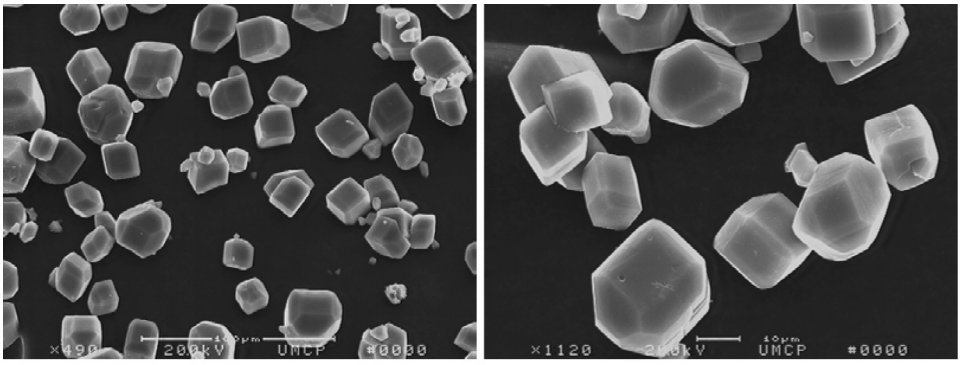

(a) (b)

Figure 1 SEM images of AlH_3.

was joule heated at very high heating rates. The system employed in this study utilized an in-house power supply capable of delivering heating rates of $\sim 6 \times 10^5$ K/s. The coated wire is then inserted within the ion-extraction region of a TOF mass spectrometer capable of scanning rates of more than 20,000 Hz ($\sim$100 μs; Zhou et al., 2009). This system was used to characterize the H_2 release temperatures, and the Arrhenius parameters for the onset of the release of hydrogen for heating rates ranging from about 7×10^4 K/s to approximately 6×10^5 K/s.

Ignition Experiments

Ignition of alane was studied for heating rates in the same range as those for hydrogen release (from $\sim 7 \times 10^4$ K/s to $\sim 6 \times 10^5$ K/s). Ignition in air, CO_2, and in O_2 diluted with various amounts of argon was monitored through broadband optical emission from the T-jump apparatus with photomultiplier tubes (PMTs).

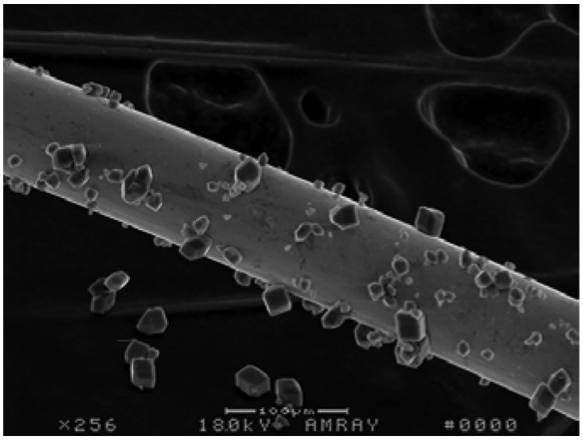

Figure 2 SEM image of AlH_3 on platinum filament.

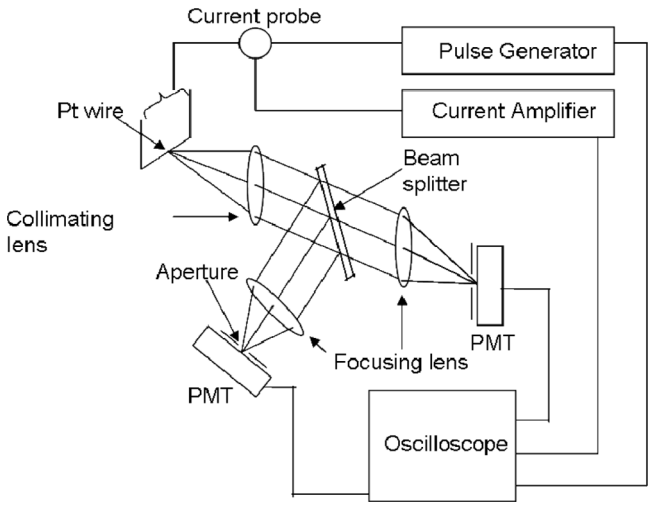

Figure 3 Schematic diagram of T-Jump optical emission system.

For the O_2/argon tests the oxygen mole fraction was adjusted from 0.05 to 0.5. Two PMTs were used to monitor broadband light emission in real time, with the output sent directly to an oscilloscope. Ignition was characterized by a sharp increase in light emission. Figure 3 provides a schematic diagram of the test setup. Similar approaches have been utilized by other researchers to characterize ignition behavior of various materials (see Schoenitz et al., 2007; Umbrajkar et al., 2006).

RESULTS AND DISCUSSION

During both the hydrogen release experiments and the ignition experiments, the input voltage and resulting current were recorded. From the recorded voltage and current, and the known length of the platinum wire, the temperature time history can be found as a function of wire resistance using the Callendar-Van Dusen equation:

$$\frac{R}{R_o} = 1 + \alpha T + \beta T^2 \tag{3}$$

Where $\alpha = 3.91 \times 10^{-3}$, $\beta = -5.78 \times 10^{-7}$, R_o is the reference resistance obtained from the length of the wire at ambient temperature.

Hydrogen Release

Figure 4 shows a typical voltage and current history for a given experiment, from which the temperature in Figure 5 is deduced. The temperature time history is generally very linear in nature, which enables a heating rate to be extracted by taking the slope of the temperature-time plot.

Figure 6 shows time-resolved mass spectrum of Alane for a heating rate of $\sim 6 \times 10^5$ K/s. The spectra observed at t = 0 ms are essentially the background signal

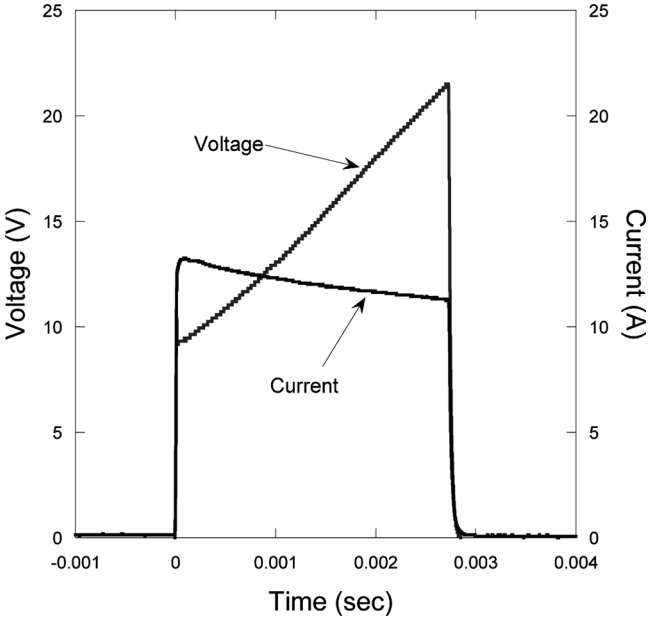

Figure 4 Typical voltage and current trace from 76 um pt wire for heating rate of $\sim 5 \times 10^5$ K/s.

and consists primarily of H_2O (m/z = 18), OH (m/z = 17), and N_2 (m/z = 28). In this particular example, the first instance of H_2 appears at t = ~1.5 ms, In Figure 7 we plot the time evolution of H_2 along with the measured wire temperature. From this

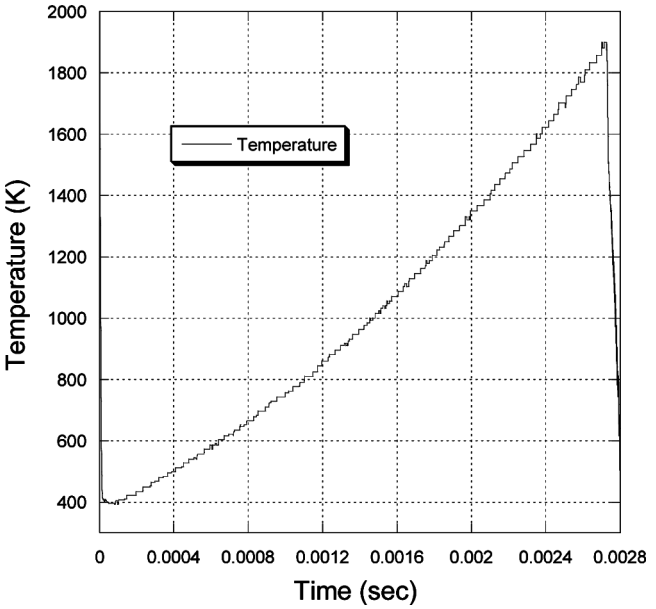

Figure 5 Typical temperature-time history for a heating rate of $\sim 5 \times 10^5$ K/s.

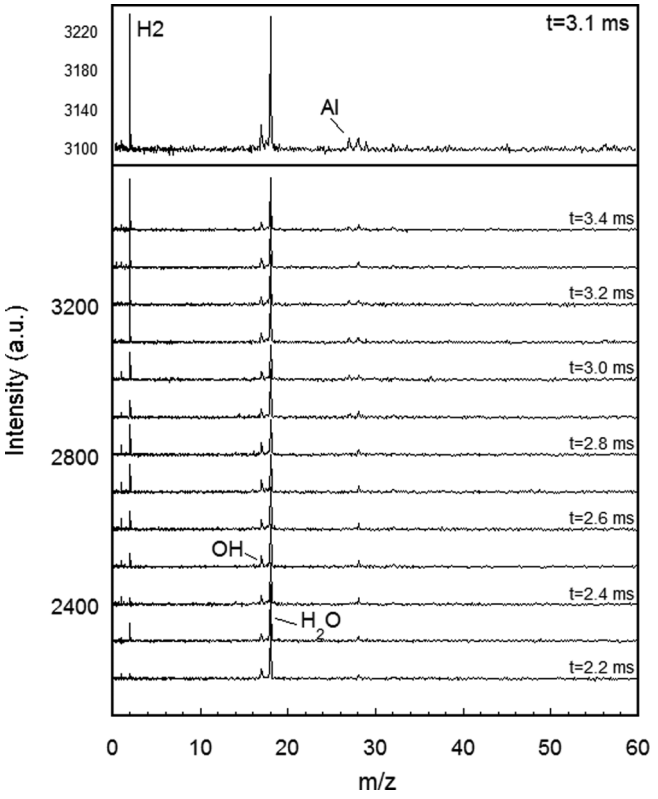

Figure 6 Temporally resolved T-Jump TOF mass spectra for a heating rate of $\sim 6 \times 10^5$ K/s.

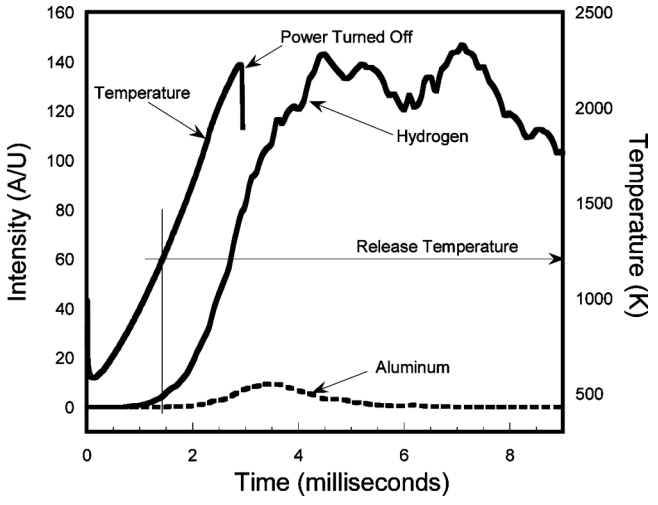

Figure 7 Hydrogen release for heating rate of $\sim 6 \times 10^5$ K/s.

it can be seen that the onset of H_2 evolution is ~1200 K. Over the full heating pulse mass spectra were collected and showed only H_2 and Al, with no evidence of aluminum oxides or suboxides, suggesting the stability of any oxide coating. From Figure 7 it can be seen that the filament was turned off after approximately 3 ms; however, it is important to understand that the filament remains hot for a relatively long time compared to the sampling duration. To make our point clear, if we consider an energy balance (Eq. [4]) on the filament in which radiation is the lone source of heat transfer for the filament (convection may be neglected since the experiments were conducted in a vacuum):

$$\rho V c \frac{dT}{dt} = -\varepsilon A \sigma (T^4 - T_{sur}^4) \tag{4}$$

Which when solved for the time to reach an arbitrary temperature, T, is (Incropera and Dewitt, 1996)

$$t = \frac{\rho V c}{4\varepsilon A \sigma T_{sur}^4} \left\{ \ln\left|\frac{T_{sur} + T}{T_{sur} - T}\right| - \ln\left|\frac{T_{sur} + T_i}{T_{sur} - T_i}\right| + 2\left[\tan^{-1}\left(\frac{T}{T_{sur}}\right) - \tan^{-1}\left(\frac{T_i}{T_{sur}}\right)\right]\right\} \tag{5}$$

Solving iteratively, we find that the temperature of the filament changes by less than 50 K in 9 ms, when the initial temperature is 1200 K. Thus, for the duration of our sampling the filament remains hot even though the power has been removed, and can continue to supply energy to the particles. This is consistent and explains why in Figure 7 we see hydrogen and aluminum after the power to the filament has been removed. One additional issue also needs to be addressed and is associated with heat transfer resistance in heating of the alane crystals. In particular, are the alane crystallites at the wire temperature? Alane is known to have a low thermal conductivity, which leads to two potential complicating issues: (a) gradients within an individual particle and (b) nonuniformity in temperature through layers of particles. Ghafir et al. (2009) pointed out that the thermal conductivity of a hydrided metal cannot be determined independently by experiment because the conductivity of hydrided metals is a strong function of the concentration of bonded hydrogen, and thus the effective conductivity changes during either absorption or desorption of hydrogen. Instead, measurements of an effective thermal conductivity of a powdered bed are typically made from which Lototsky (2008) extracted a value of $0.35\,W/[m * K]$. In order to examine the effects of the low thermal conductivity of alane, we have conducted a 1D analysis for particle heating, using the Lototsky value for the thermal conductivity, and the values for specific heat given by Sinke et al. (1967), at our highest heating rate ($\sim 6 \times 10^5$ K/s) to calculate the thermal diffusivity, α. In our analysis we assumed that the only mode of heat transfer was conduction through the particle. At the interface of the filament-particle interface we assume the particle is at the wire temperature (i.e., $T[0, t] = T_{wire}$), and at the particle-air interface an insulating boundary condition (i.e., $dT/dx[x = L] = 0$). With these

boundary conditions we solve an energy balance numerically for a range of particle sizes found in this study.

$$\frac{dT}{dt} = \alpha \frac{\partial^2 T}{\partial x^2} \tag{6}$$

For this model system we found that for a 5 μm particle, the temperature difference across the particle is no more than 40 K. As this temperature variation is within the uncertainty in our wire temperature measurement, we may reasonably conclude, that at least for particles on the lower end of the particle size distribution, particles are at the wire temperature prior to ignition. For the larger particles in our size distribution the thermal gradients within an individual particle become significant.

Figure 8 shows the hydrogen release temperature of alane as a function of heating rate. The hydrogen release temperature was selected as the first instant at which the mass spectrometer detected H_2. Given our previous discussion of temperature effects of intraparticle temperatures it should be expected that our release temperature is biased toward the smallest particles in our size distribution, and those particles that are in direct contact with the filament. As the figure shows, the release temperature clearly increases from about 650 to about 1100 K as the heating rate increases from 7×10^4 to 6×10^5 K/s. Bazyn et al. (2004), on the other hand, observed hydrogen desorption at lower temperatures of 400–500 K. Similarly, Ismail and Hawkins (2005) found that alane decomposition began around 400 K for a heating rate of 0.5°C/min and increased to about 450 K at a heating rate of 20°C/min.

To process our results we employed the Ozawa (1965, 1970) isoconverison method to extract Arrhenius parameters for hydrogen release. A similar approach

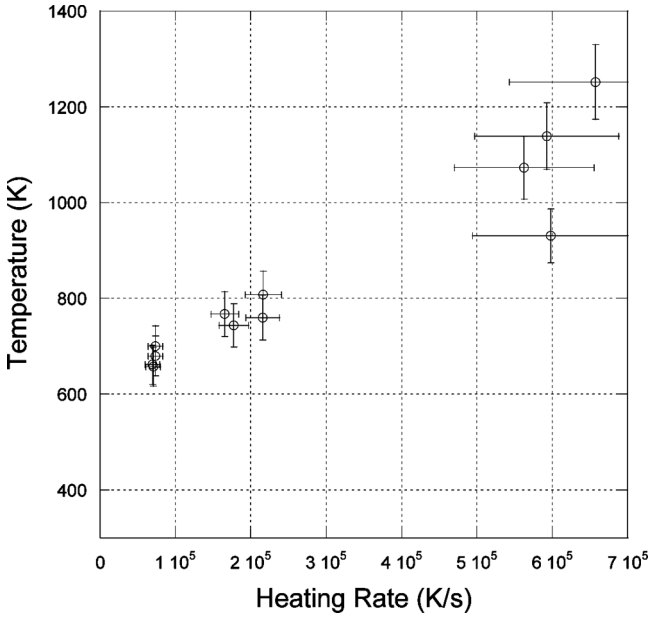

Figure 8 Hydrogen release temperature from AlH_3 as a function of heating rate.

was used by Schoenitz et al. (2007) in describing a thermite reaction with ignition data as well as data from the onset of heat flow in a Differential Scanning Calorimeter (DSC). In order to employ this method to the present study the natural logarithm of the heating rate, β, was plotted against the reciprocal of the hydrogen release temperature, $1/T_{H2r}$, from which the slope can be used to extract the activation energy Ea.

$$\ln(\beta) = const - \frac{E_a}{R_u T} \tag{7}$$

Figure 9 shows the results of application of the Ozawa (1965, 1970) method. For the heating rates in our study, $\sim 7 \times 10^4 < \beta < \sim 6 \times 10^5$, the activation energy found for hydrogen release was $\sim$27.3 kJ/mol. In contrast Ismail and Hawkins (2005) and Bazyn et al. (2004) found activation energies that were several times larger. For instance Bazyn et al. (2004) determined that the activation energy for the 90% decomposition time was approximately 97 kJ/mol, which was similar to the activation energy determined by Ismail and Hawkins (2005) in their single-step analysis. For consistency we have also plotted Ismail and Hawkins's (2005) data in Figure 9 using the Ozawa method based on the onset of hydrogen evolution. In doing so we found the activation energy to be nearly identical (96 kJ/mol compared to 97 kJ/mol) to Ismail and Hawkins's (2005) one-step approach. In a two-step model, in which the first step describes a *n*th-dimensional nucleation or growth reaction, and the second step could be described by a typical chemical reaction or by

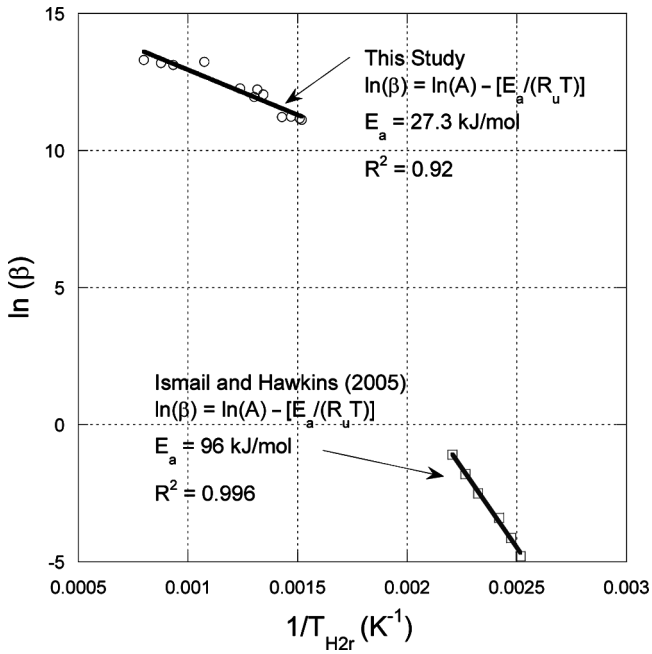

Figure 9 Arrhenius plot of AlH_3 hydrogen release.

another Kolmogorov-Johnson-Mehl-Avrami (KJMA) equation, the activation energies ranged from ~84 to 99 kJ/mol for the first step and ~63 to 89 kJ/mol for the second step (Ismail and Hawkins, 2005). To explain the discrepancy in our activation energies with prior results we note a major difference between the prior studies (Bazyn et al., 2004; Ismail and Hawkins, 2005) and our work is the heating rate. Bazyn et al.'s (2004) study used a constant temperature, whereas Ismail and Hawkins's (2005) highest heating rate was only 20°C/min. The minimum heating rate in this study was 5 orders of magnitude higher than that of Ismail and Hawkins's (2005). In contrast to all these experimental results, Ojwang et al.'s (2009) computational study gives an Al-H bond energy of ~390 kJ/mol. Assuming that hydrogen release from alane actually goes through a concerted reaction to release molecular hydrogen, they find for Al_2H_6 decomposition, an activation barrier of ~230 kJ/mol. On the other hand these studies found that for $Al_{28}H_{84}$ that the early stages of hydrogen desorption from the larger cluster were exothermic, and that as more hydrogen was desorbed, the process eventually transitions to an endothermic process with desorption energies of ~30 kJ/mol. This result implies that there is a continuous change in material properties as the extent of desorption continues.

Arrhenius plots are quite useful in that changes in activation energy in different temperature regimes imply changes in mechanism. In our case our high heating rate experiments apparently push the kinetics into a much higher temperature regime, and where another mechanism of hydrogen evolution is controlling. The previous research on alane that we have cited (Bazyn et al., 2004; Ismail and Hawkins, 2005) was conducted at much lower heating rates and as a consequence at lower temperatures. As Thomas and Thomas (2005) explained, at low temperatures high activation energy chemically controlling processes are observed, whereas transport processes that have smaller activation energies dominate at higher temperatures. Thus when transitioning from a chemically controlled process at low temperatures to a diffusion controlled process at high temperatures, an Arrhenius plot typically shows a change in slope that is one-half ($E_a/2R$) the low-temperature activation energy. As the temperature is increased even further, mass transfer through the gas phase from the fluid to the solid becomes rate controlling. Because the mass transfer coefficient is only a weak function of temperature the apparent activation energy can be even less than half of the true activation energy (Thomas and Thomas, 2005). The activation energy in our study was found to be about one third of the previously published values. This would suggest that at the high heating rates used in our experiments, the intrinsic chemical kinetics of hydrogen dissociation within the crystal is sufficiently fast that our temperature dependent observations are really probing the kinetics of hydrogen transport though the crystal.

To test the reasonableness of this hypothesis we make the following scaling argument. Young and Scully (1998) determined the diffusion of hydrogen in aluminum to be from 1×10^{-5} to 1×10^{-6} cm^2/s for the temperature range of interest to the present study. If considering the diffusion of hydrogen through aluminum as a potential rate limiting mechanism, and perform a simple scaling analysis, L^2/D, it is possible to obtain time scales on the order of milliseconds on the lower end, which is consistent with the time scales we observe. Assuming Ojwang et al. (2009) $Al_2H_6 \geq Al_2H_4 + H_2$ as a reasonable representation of a concerted unimolecular elimination of H_2 we can assign a pre-exponential factor by analogy to similar

gas-phase reactions of $\sim 10^{13}\,s^{-1}$ (Benson, 1976). Rather than using the 230 kJ/mol activation energy obtained by Ojwang et al. (2009) we get a characteristic reaction time of less than 1 ms, and thus shorter than our experimental observation. The 230 kJ/mol value is probably on the high end because matrix effects usually lower activation energies of bond breaking events in condensed phases. This implies that our experiments should be probing hydrogen transport within the AlH_x matrix so long as activation energies for the intrinsic kinetics are on the order of 200 kJ/mol or lower.

Ignition Experiments

Ignition of alane was studied in air, CO_2, and with O_2 diluted with argon such that the mole fraction of oxygen ranged from 0.05 to 0.5. Ignition of alane in air is of interest for a variety of uses, but particularly as a fuel in an air-breathing propulsion system. CO_2 is of interest because along with H_2O it is one of the primary oxidizers for fuel supplements in solid rocket motors using composite (AP-based) propellants. Experiments were run in an oxygen–argon environment in order to determine a critical O_2 concentration required for ignition. Figure 10 shows a typical optical emission profile during an ignition experiment. In each case a background shot was taken and subtracted from the signal and smoothed to aid in data interpretation. Typically, the signal from an ignition experiment was a factor of at least 20 times stronger than the background shot (i.e., heated wire with no coating). As the figure shows, upon heating of the wire, there is a sharp rise and subsequent fall of broadband light emission

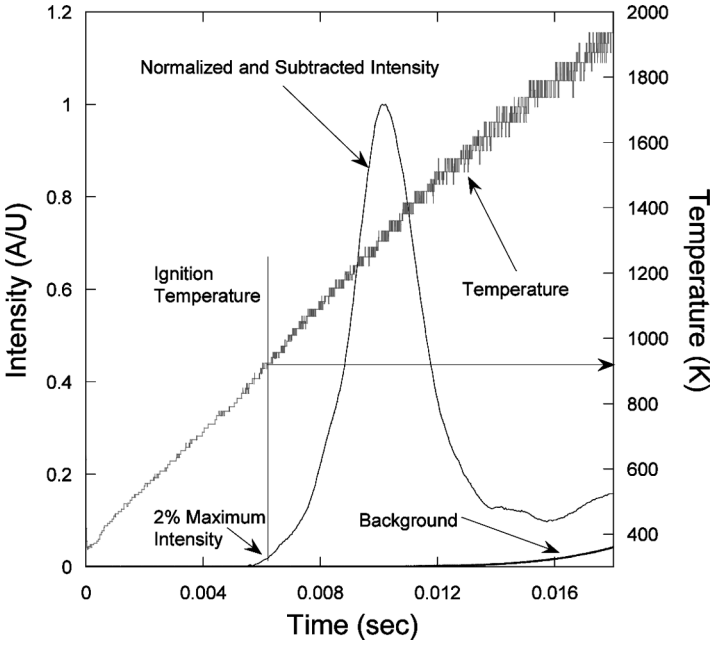

Figure 10 Example of the temporal temperature and optical emission for an AlH_3 ignition event.

consistent with ignition and subsequent combustion of the particle. We have defined the point of ignition as being 2% of the maximum signal intensity as an unambiguous and consistent identifier.

Figure 11 plots the ignition temperature as a function of heating rate and clearly shows that within experimental uncertainty, there is no difference in the ignition temperature in air or CO_2. In both cases the ignition temperature increases as the heating rate increases starting from just below the melting temperature of aluminum (933 K), at the lowest heating rate, to about 1500 K at the highest heating rate. Interestingly, the same experiments, repeated in air for similar sized micron-scale aluminum, does not result in ignition. Typically, micron-sized aluminum particles require a temperature of 2000 K or more to achieve ignition (Brossard et al., 1997; Brzustowski and Glassman, 1964; Friedman and Macek, 1962, 1963; Kuehl, 1965) and is typically associated with the damage to the oxide shell (Price, 1983), with the ignition temperature approaching the melting point of alumina (~2300 K). With alane igniting at much lower temperatures it is clear that the ignition mechanism is very different. In our mass spectrometer measurements we never detected any aluminum oxide or suboxides, which has been observed in the heating of nanoaluminum (Zhou et al., 2009). Similarly, Energy Dispersive X-Ray Spectroscopy (EDX) analysis only revealed elemental aluminum (hydrogen cannot be detected using EDX). These results suggest that there may not be any significant oxide, or if there is an oxide shell the damaging mechanism must be different, such that molten aluminum becomes exposed to oxidizing species at much lower temperatures. One possibility is that the evolving hydrogen places sufficient stress on the oxide to expose the underlying aluminum.

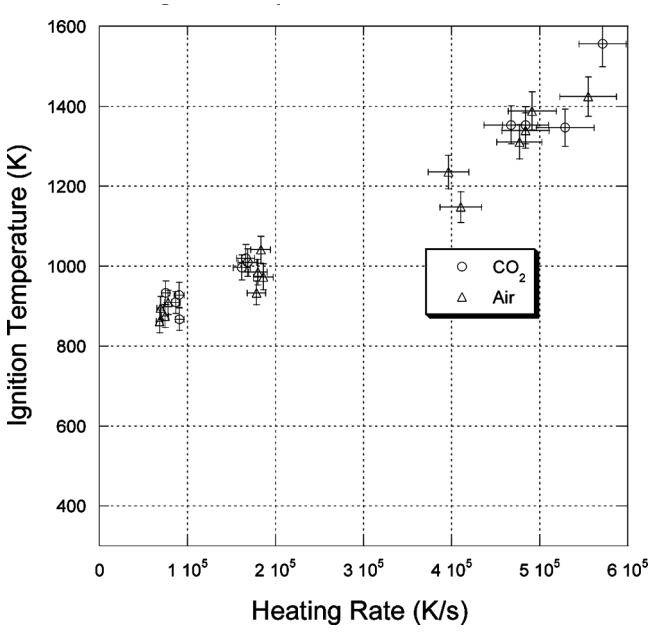

Figure 11 Ignition temperature of AlH_3 in air and CO_2 as a function of heating rate.

Nanosized aluminum has been found to ignite at far lower temperatures (Bazyn et al., 2006) and close to those found in this study. The increases in burning rate found in gelled nitromethane (Weiser et al., 2007) and Ammonium Perchlorate/HTPB propellants (Deluca et al., 2007) compared to similarly aluminized versions may potentially be attributed directly to the lower ignition temperature of alane. Because the alane would ignite at less than half of the temperature that standard micron-sized aluminum would, it would ignite much closer to the surface of a solid propellant in a rocket motor, thereby increasing the heat feedback to the propellant surface, which would in turn increase the burning rate. A similar phenomenon was observed with nanosized aluminum (Risha et al., 2003).

Once again, the Ozawa method (Ozawa, 1965, 1967) was used to extract the Arrhenius parameters of the ignition process. As Figure 12 shows, the activation energy is approximately the same ($\sim$37 kJ/mol) for the ignition process in both air and CO_2.

The dependence of ignition on oxygen concentration was also studied, the results of which can be seen in Figure 13. Ignition was studied in an oxygenated environment by diluting O_2 with varying amounts of argon ranging from 5% O_2 up to 50% O_2 by mole. During this part of the study only the slowest heating rate ($\sim 7 \times 10^4$ K/s) was selected for testing. No ignition was obtained for experiments in which the oxygen concentration was 5% by mole. The average ignition temperature in CO_2(solid line) and air (dashed line) was also plotted in Figure 13 for comparison and the error bars represent one standard deviation of the respective

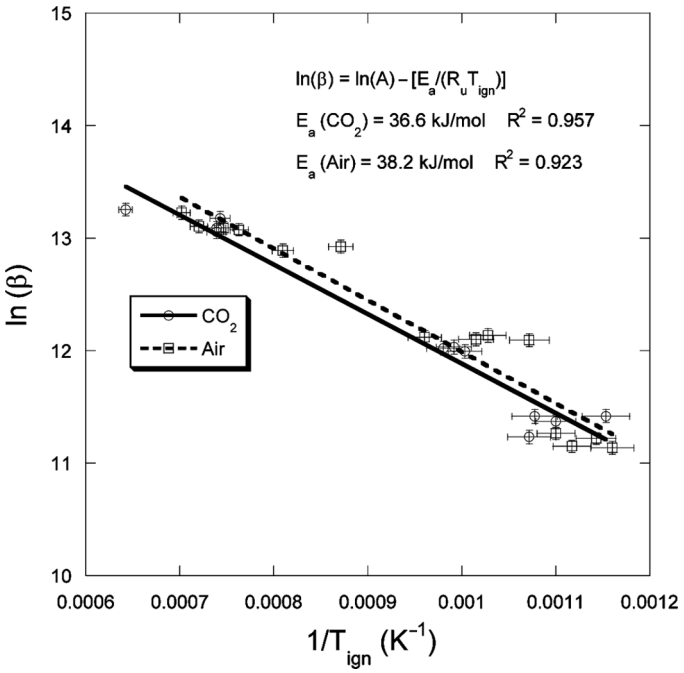

Figure 12 Arrhenius plot based on the heating rate, β, for AlH_3 ignition in air and CO_2.

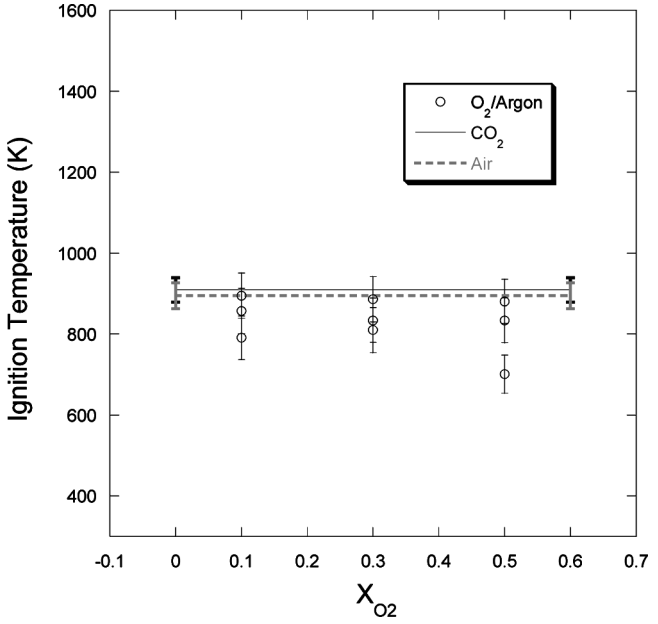

Figure 13 Ignition temperature of AlH_3 in Ar/O_2 Mixtures for a heating rate of $\sim 7 \times 10^4$ K/s.

measurements. As Figure 13 shows, the ignition event is fairly insensitive to oxygen concentration within the ranges under consideration. With the exception of an outlier at each extreme ($X_{O2} = 0.1$ and 0.5) condition, within measurement error all the ignition data in the oxygen–argon environment falls within the standard deviation bands of the CO_2 and air experiments. This result coupled with the ignition results in air and CO_2 suggest that the ignition of alane is primarily determined by thermal–physical behavior, provided that a sufficient oxidizer is available.

Figure 14 shows the temporal profiles in optical emission as a function of oxygen concentration and provides a view of the overall combustion times. As the O_2 concentration increases, the PMT traces show much faster rise times and a shorter temporal emissive period compared to the very broad profile at $X_{O2} = 0.1$. These profiles demonstrate that although ignition may be insensitive to oxidizer concentration, once ignition occurs the combustion process is far more vigorous at the higher oxygen concentrations, which would be expected. For comparative purposes, the 50% full width half maximum (FWHM) burning time has been plotted in Figure 15. The data represent the average burning time of three experiments at each oxygen concentration, and the error bars represent the standard deviation in the data. The relatively large error bars, particularly at the two higher oxygen concentrations, demonstrate the difficulty in applying to the wire the same amount of material with a uniform coating and the relatively wide size distribution of particles in this sample. Nevertheless, a clear linear trend whereby burning time is increased by a factor of approximately three when the O_2 concentration is reduced from $X_{O2} = 0.5$ to $X_{O2} = 0.1$. It should be noted that Bazyn et al. (2007) found that the burning times of alane were virtually identical to that of aluminum of the same size. Application of

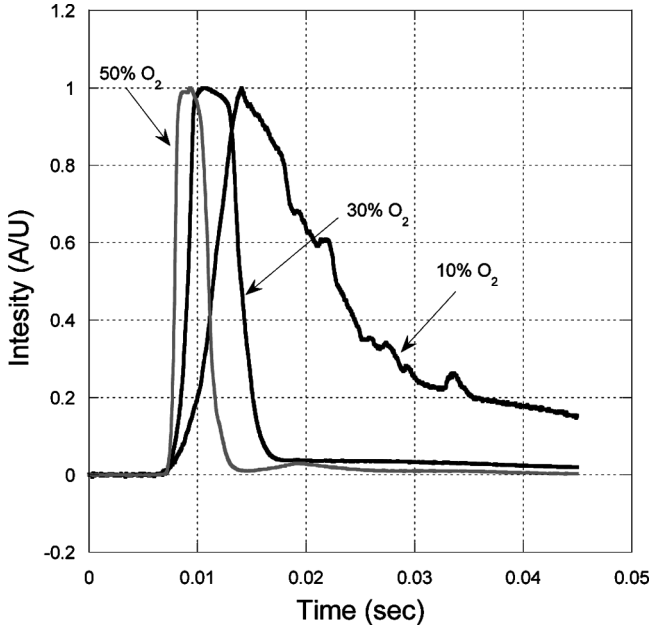

Figure 14 Temporal optical emission of combustion for various O_2 concentrations for a heating rate of $\sim 7 \times 10^4$ K/s.

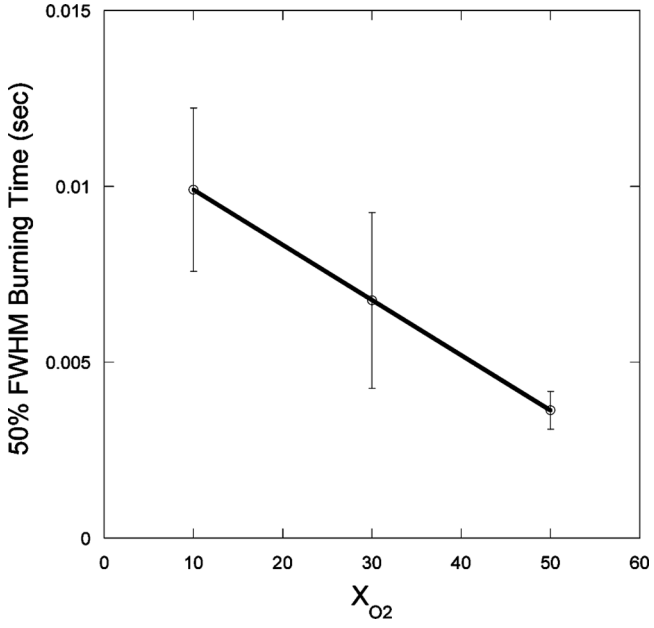

Figure 15 Burning time of AlH_3 as a function of O_2 concentration for a heating rate of $\sim 6 \times 10^4$ K/s.

Beckstead's (2005) correlation suggests that the burning times should be reduced by a factor of 5 when changing the oxygen fraction from 0.1 to 0.5. However, Beckstead's correlation is intended to describe the burning time of a single particle. In this case we have a group of particles, some of which are likely to be agglomerated, perhaps heavily, which do not necessarily all ignite at the same time. Care should be taken in interpreting these results, as they are not meant to identify burning times of single particles, but rather to display the trend in the combustion behavior.

CONCLUSION

The ignition behavior of α-AlH3 was studied by investigating two separate components of the ignition process. First, the hydrogen release behavior was studied by a T-jump TOF mass spectrometer. The onset of hydrogen release was characterized through a heating rate range of $\sim 7 \times 10^4$ to $\sim 6 \times 10^5$ K/s. It was found that the hydrogen release onset temperature had a clear dependence on heating rate, which increased with heating rate with an activation energy of 27.3 kJ/mol, and was considerably below that found in other investigations. This difference was attributed to the much higher heating rates used in this study. This results in probing a higher temperature regime, for which the observed lower activation energy implies that the rate controlling process is not the intrinsic kinetics of Al-H bond breaking but rather an intraparticle diffusion limit.

Ignition temperatures were significantly lower than that found for traditional micron-sized aluminum particles, and was more representative of ignition temperatures of nanoaluminum. Ignition of the alane particles in air, CO_2, and in O_2/argon mixtures was found to be very sensitive to heating rate and ranged from 900–1500 K, and was independent of the atmospheric composition. The activation energy was approximately 37 kJ/mol in both air and CO_2.

ACKNOWLEDGEMENTS

This research effort was sponsored through Center for Energetic Concepts Development (CECD), a collaborative effort between the Naval Surface Warfare Center–Indian Head Division (NSWC-IHD), and the University of Maryland, College Park (UMD). Partial support was also obtained from the Army Research Office (ARO) and the Defense Threat Reduction Agency (DTRA).

NOMENCLATURE

A	Filament surface area
c	Filament specific heat
dt	Differential time
dT	Differential temperature
E_a	Activation energy
k	Particle thermal conductivity
R	Resistance
R_o	Reference resistance
R_u	Universal gas constant

t time
T Temperature
T_i Initial temperature
T_{sur} Temperature of surroundings
V Filament volume
X_{O2} Oxygen mole fraction
α Thermal diffusivity of the particle
β Heating rate
ε Filament emissivity
ρ Filament density
σ Boltzman's constant
∂x Differential spatial coordinate

REFERENCES

Bazyn, T., Eyer, R., Krier, H., and Glumac, N. 2004. Combustion characteristics of aluminum hydride at elevated pressure and temperature. *Journal of Propulsion and Power*, **20**, 427–431.

Bazyn, T., Krier, H., and Glumac, N. 2006. Combustion of nanoaluminum at elevated pressure and temperature behind reflected shock waves. *Combustion and Flame*, **145**, 703–713.

Bazyn, T., Krier, H., Glumac, N., Shankar, N., Wang, X., and Jackson, T.L. 2007. Decomposition of aluminum hydride under solid rocket motor conditions. *Journal of Propulsion and Power*, **23**, 457–464.

Beckstead, M.W. 2005. Correlating aluminum burning times. *Combustion, Explosives, and Shockwaves*, **41**, 533–546.

Benson, S.W. 1976. *Thermochemical Kinetics*, 2nd ed., Wiley Interscience, New York.

Brossard, C., Ulas, A., Yen, C.L., and Kuo, K.K. 1997. Ignition and combustion of isolated aluminum particles in the post-flame region of a flat-flame burner. 16th International Colloquium on the Dynamic Explosions and Reactive Systems, Krakow, Poland.

Brzustowski, T.A., and Glassman, I. 1964. Spectroscopic investigation of metal combustion. *Prog. Astronaut. Aeronaut.*, **15**, 75.

Deluca, L.T., Galfetti, L., Severini, F., Rossettini, L., Meda, L., Marra, G., D'Andrea, B., Weiser, V., Calabro, M., Vorozhtsov, A.B., Glazunov, A.A., and Pavlovets, G.J. 2007. Physical and ballistic characterization of AlH3-based space propellants. *Aerospace Science and Technology*, **11**, 18–25.

Friedman, R., and Macek, A. 1962. Ignition and combustion of aluminum particles in hot ambient gases. *Combustion and Flame*, **6**, 9–19.

Friedman, R., and Macek, A. 1963. Combustion studies of single aluminum particles. *Proc. Comb. Instit.*, **9**, 703–709.

Gal'chenko, Y.A., Grigor'ev, Y.M., and Merzhanov, A.G. 1973. Ignition of aluminum in carbon dioxide. *Combustion, Explosions, and Shockwaves*, **9**, 96–98.

Ghafir, M.F.A., Batcha, M.F.M., and Raghavan, V.R. 2009. Prediction of the thermal conductivity of metal hydride—The inverse problem. *International Journal of Hydorgen Energy*, **34**, 7125–7130.

Graetz, J., and Reilly, J.J. 2005. Decomposition kinetics of the AlH_3 polymorphs. *Journal of Physical Chemistry B*, **109**, 22181–22185.

Graetz, J., and Reilly, J.J. 2006. Thermodynamics of the a, b, and g polymorphs of AlH_3. *Journal of Alloys and Compounds*, **424**, 262–265.

Graetz, J., Reilly, J.J., Kulleck, J.G., and Bowman, R.C. 2007. Kinetics and thermodynamics of the aluminum hydride polymorphs. *Journal of Alloys and Compounds*, **446–447**, 271–275.

Il'in, A.P., Bychin, N.V., and Gromov, A.A. 2001. Products of combustion of aluminum hydride in air. *Combustion, Explosion, and Shock Waves*, **37**, 490–491.

Incropera, F.P., and DeWitt, D.D. 1996. *Fundamentals of Heat and Mass Transfer*, Wiley, New York.

Ismail, I.M.K., and Hawkins, T. 2005. Kinetics of thermal decomposition of aluminum hydride: I-non-isothermal under vacuum and in inert atmosphere (argon). *Thermochimica Acta*, **439**, 32–43.

Kuehl, D.K. 1965. Ignition and combustion of aluminum and beryllium. *AIAA Journal*, **3**, 2239–2247.

Lototsky, M.V., Klochko, Y.V., Ryabchikov, D.L., and Ershova, O.G. 2008. Heat transfer performances of AlH3 composites with recompressed thermal expanded graphite. INTAS Meeting—Institute of Solid State Physics, Chernogolovka, Russia.

Ojwang, J.G.O., van Santen, R.A., Jan Kramer, G., van Duin, A.C.T., and Goddards, W.A. 2009. Parameterization of a reactive force field for aluminum hydride. *J. Chem. Phys.*, **131**, 044501.

Ozawa, T. 1965. A new method for analyzing thermogravimteric data. *Bull. Chem. Soc. Japan*, **38**, 1881.

Ozawa, T. 1970. Kinetic analysis of derivative curves in thermal analysis. *Journal of Thermal Analysis*, **2**, 301.

Petrie, M.A., Bottaro, J.C., Schmitt, R.J., Penwell, P.E., and Bomberger, D.C. 2001. *U.S. Patent No. 6,228,338*. U.S. Patent and Trademark Office, Washington, DC.

Price, E.W. 1983. Combustion of metallized propellants. *Prog. Astronaut. Aeronaut.*, **90**, 479–513.

Risha, G.A., Evans, B.J., Boyer, E., Wehrman, R.B., and Kuo, K.K. 2003. Nano-sized aluminum and boron-based solid fuel characterization in a hybrid rocket engine. 39th AIAA/ASME/SAE/ASEE Joint Propulsion Conference, Huntsville, AL, USA, AIAA 2003-4593.

Schoenitz, M., Umbrajkar, S., and Dreizin, E.L. 2007. Kinetic analysis of thermite reactions in Al-MoO_3 nanocomposites. *Journal of Propulsion and Power*, **23**, 683–687.

Sinke, G.C., Walker, L.C., Oeting, F.L., and Stull, D.R. 1967. Thermodynamic properties of aluminum hydride. *Journal of Chemical Physics*, **47**, 2759–2761.

Thomas, J.M., and Thomas, W.J. 2005. *Principles and Practices of Heterogeneous Catalysis*, VCH, New York.

Umbrajkar, S., Schoenitz, M., and Dreizin, E.L. 2006. Exothermic reactions in Al–CuO nanocomposites. *Thermochimica Acta*, **451**, 34–43.

Weiser, V., Eisenreich, N., Koleczko, A., and Roth, E. 2007. On the oxidation and combustion of AlH_3 a potential fuel for rocket propellants and gas generators. *Propellants, Explosives, Pyrotechnics*, **32**, 213–221.

Young, G.A., and Scully, J.R. 1998. The diffusion and trapping of hydrogen in high purity aluminum. *Acta Materialia*, **46**, 6337–6349.

Zhou, L., Piekiel, N., Chowdhury, S., and Zachariah, M. 2009a. T-Jump/time-of-flight mass spectrometry for time-resolved analysis of energetic materials. *Rapid Communications in Mass Spectrometry*, **23**, 194–202.

Zhou, L., Piekiel, N., Chowdhury, S., and Zachariah, M.R. 2009b. T-jump/Time-of-flight mass spectrometry for time resolved analysis of fast condensed stated reactions. 47th Aerospace Sciences Conference and Exhibit, Orlando, FL, USA, AIAA 2009-639.